

## Assessing spatial-temporal trends of ceaf rainfall during ond season

Kelly Dusabe<sup>1\*</sup>, Ling Zhang<sup>1,2</sup>

<sup>1</sup>School of Atmospheric Science, Nanjing University of Information Science and Technology, Nanjing 210044, China

<sup>2</sup>Collaborative Key Laboratory of Meteorological Disaster, Nanjing University of Information Science and Technology, Nanjing, China

\*Corresponding author: Kelly Dusabe, School of Atmospheric Science, Nanjing University of Information Science and Technology, Nanjing 210044, China, Tel: +86 175 5887 5894; E-Mail: [kellykaleche@yahoo.com](mailto:kellykaleche@yahoo.com)

Received: April 24, 2021; Accepted: May 12, 2021; Published: June 28, 2021

### Abstract

In Central East Africa (CEAF) and Africa, Precipitation plays a vital role by controlling agriculture production because of the traditional techniques used, which relies totally on rainfall. The present study aims at showing the spatial-temporal characteristics of rainfall over CEAF from 1981 to 2016. The analysis was conducted based on the CHIRPS dataset after evaluation and comparison against the observational data on around 48 synoptic stations. The spatial and temporal distribution from the empirical orthogonal function was revealed through the first EOF's dominant principal components (PC1) and explained 60% of the total variance. It showed five-strong wet years (1982, 1997, 2006, 2011) and dry years (1987, 1993, 1996, 2005). The study conducted a series of trend analyses of the OND (October-December) season and interannual precipitations, which reveal slight decrease slopes during the studied 36 years. Sequential Mann-Kendall test was employed and depicted an abrupt change in the historical data during OND season, while a slight decrease trend at the interannual timescale was shown. The wavelet power spectrum (WPS) test was also employed to characterize the precipitation cycle and possible periodicity. The test revealed the years of strong signals in the region to be 1996, 1997, 1998, 2002, 2006, which concur with the PC1 results.

**Keywords:** CEAF; trend; periodicity; rainfall variability

### Introduction

Climate change and variability in the weather present undeniable challenges, affecting ecosystems and biodiversity, and people in the foreseeable future, as reported by [1]. As a result of global warming, there are indications that rain patterns are already changing globally[2]. Various aspects of climate variability and climate change are studied in East Africa, focusing on rainfall, as opposed to temperature[3]. This result is due to the importance of rain in the tropics, as reported by ]. In his study on Global observed long-term changes in temperature and precipitation extremes concerning the

variability in rainfall patterns, [5] said some regions reporting periods of excess rainfall, while others report periods of decline.

During the past several decades, research agendas have concentrated on the detection and attribution of climate variation and monitoring climate change and climate variability[6]. This is due to concerns about global warming, rising demand for water, and economic growth, and the role of water in natural disasters such as floods, droughts, and severe erosion [7]. Africa's lack of economic growth and institutional capacity makes it particularly vulnerable to the impacts of climate change. The recent extreme weather events in the Africa Great Lakes Region have increased concerns regarding the future sustainability of socio-economic development and agriculture and water resources. Farming is the primary source of national income in different countries [8,9]. Agriculture is primarily crop-based and is usually rain-fed, while fishing supports large and numerous populations living around the lakes. Rainfall and temperature trends can be determined at various scales, including local or ground-based measurement, regional, and global.

Regionally, the spatial-temporal rainfall variability is indeed interconnected with large-scale climatic forces and oceanic drivers influencing the local and global scales [10-12]. The Indian Ocean Dipole (IOD) and the El-Nino Southern Oscillation are the prominent oceanic influencers of rainfall variability in the region. However, the significant large-scales alone cannot explain the variability of either rainfall or the extreme events (floods/droughts) that occurred in the area in the past decades. Previous studies have reported numerous systems that have contributed significantly to the outcome observed in the region. The short rains are highly connected to the zonal vertical circulation cell in the central equatorial Indian Ocean, referred to as Walker-type circulation [13–15] . The disturbance of this cell's normal state, which consists of upper-level easterlies and low-level westerlies over central Indian, completes the walker cell circulation[16]. Changes in sea surface temperature (SST) in the Indian Ocean pool induce the strengthening or weakening of the Walker cell, hence modulating the short rains. Therefore, IOD is closely linked to the short-ins variability and has been reported as the primary influencer. Besides, the short rains are affected by numerous other local features such as lakes, very complex topography, the Congo basin [17],jet streams [18], monsoons, quasi-biennial oscillation, sub-tropical highs, and the ITCZ [19].

This study, therefore, employs reanalysis datasets evaluated and compared to station data and different statistical methods to understand the characteristics of Spatio-temporal trends and periodicity of seasonal and annual precipitations over CEAF. This study is critical because precipitation variability is a key to solving the most significant problem that the agricultural society faces, emphasizing the essential role of agriculture in the region. This paper will be sectioned in the following order: Section 2 describes, section 2 introduces the data and methods used in the study and a description of the study domain's climatic features and topography, section 4 captures the results section 5 highlights the conclusions.

## **Datasets and methods**

### **Study Domain**

CEAF (hereafter the region between 27°E–40°E and -12°S–4°N), covers five countries: Kenya, Tanzania, Uganda, Rwanda, and Burundi[FIG.1]. CEAF borders the IO in the east, the Congo Basin in the west, Ethiopia's highlands, Somalia and South Sudan in the North, Zambia and Malawi in the South. The region has a complex relief varying from

sea level to the highest altitude. This topographical range (from 0m - 5,895m) is symbolic of an area of a highly diverse environment. It is also referred to as the African Great Lakes region because of the large water bodies that enclose it. Lakes Victoria and Tanganyika are Africa’s most extensive and deepest freshwaters. The region’s climate varies according to location, altitude, water bodies, and vegetation. Therefore, it exhibits different types of climate, including Equatorial climate experienced around Lake Victoria, Semi-Arid and Arid Climate experienced in Northern Kenya, North-eastern Uganda, and Moist Tropical Climate experienced much in Uganda territory, Alpine Climate shared around all mountains peaks. Both global climate and local factors influence rainfall in the region.

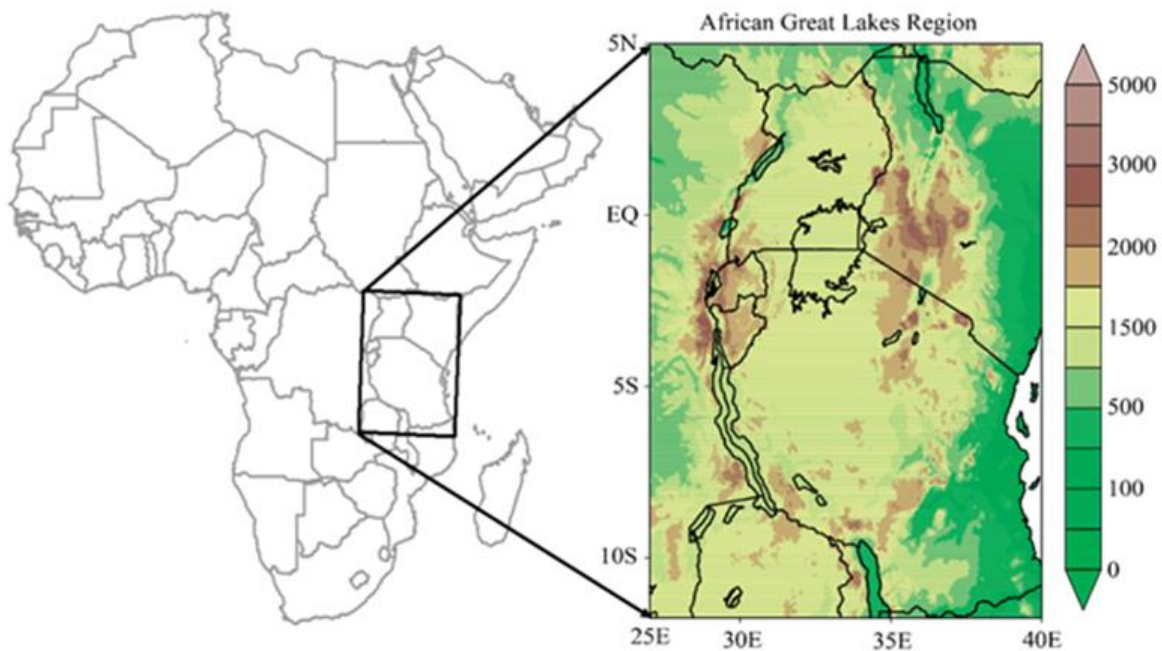


**FIG. 1. Map of Africa of the study area.**

## Datasets

### Station Datasets

Monthly station data from 48 different synoptic stations were used [TABLE 1][FIG.2.] This study used monthly data from 1981-2016 obtained from three Meteorological Agencies. The agencies include Burundi, also “named” (R1), Rwanda (R2) as well as Uganda (R3) in this study acquired from the Burundi Geographical Institute (IGEBU), Rwanda Meteorology Agency (RMA), and Uganda National Meteorological Authority (UNMA). The distribution of these stations is as shown in [FIG.2].

Although the ground-based rainfall dataset is the most accurate, the long-term deficiency or non-existent observation networks worldwide and most especially over the study area [FIG.1.] make them problematic. Therefore, we introduced satellite-based rainfall products and other observational gridded datasets as an alternative to station data. The collected station observations are used in the present study to validate the satellite product and gridded observational datasets.

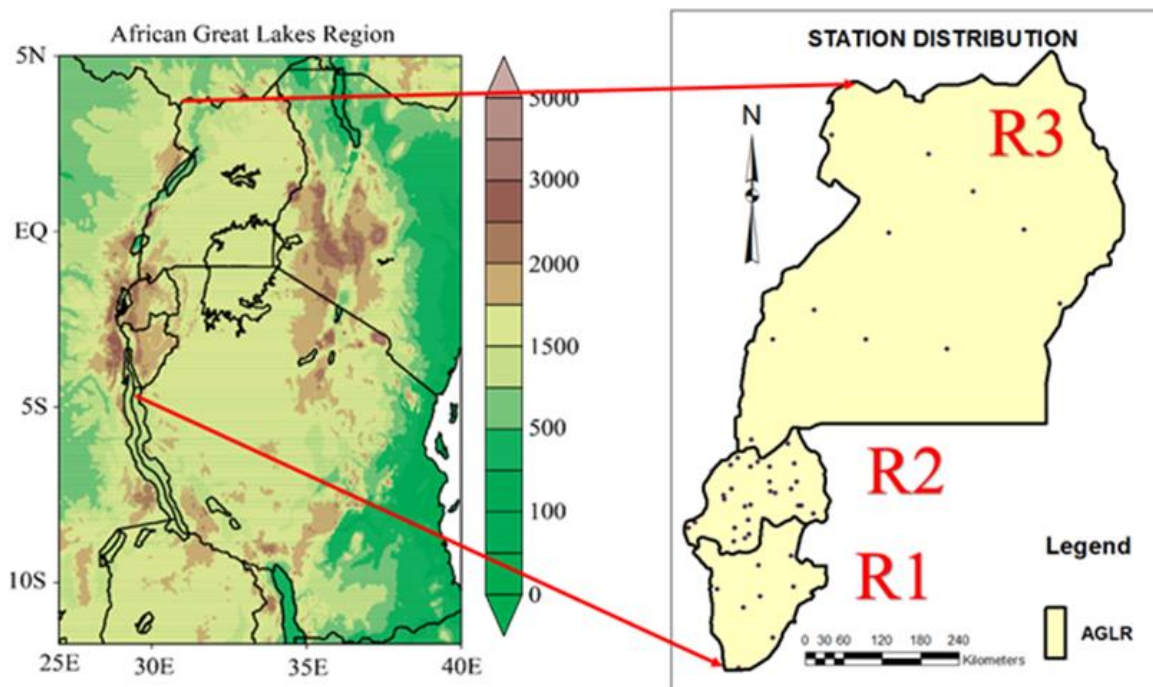


FIG 2. Coverage of weather stations in R1, R2 and R3.

TABLE 1 List of stations by country and geographical coordinates.

Country	Station	Longitude (°E)	Latitude (°)
<b>Burundi</b>	Buja	29.32	-3.32
	Gitega	29.92	-3.42
	Cankuzo	30.38	-3.28
	Gisozi	29.68	-3.57
	Muyinga	30.35	-2.85
	Musasa	30.1	-4
	Nyanza-lac	29.62	-4.42
<b>Rwanda</b>	Butare	29.71	-2.6
	Byimana	29.71	-2.16
	Byumba	30.05	-1.6
	Gabiro	30.4	-1.55
	Gihinga	29.9	-2.98
	Gikongoro	29.56	-2.46
	Gisenyi	29.25	-1.66
	Gitega	30.06	-1.95
	Kamembe	28.91	-2.46
	Kawangire	30.43	-1.81
	Kibeho	29.55	-2.65
	Kibungo	30.5	-2.15

	Kigali	30.13	-1.965
	Kirehe	30.66	-2.26
	Musha	30.35	-1.91
	Mushubati	29.41	-2
	Nemba	29.78	-1.6
	Nyagatare	30.31	-1.28
	Nyamata	30.45	-2.15
	Nyange	29.52	-1.91
	Nyanza	29.75	-2.35
	Rubengera	29.42	-2.06
	Ruhengeri	29.61	-1.48
	Rutongo	30.05	-1.81
	Rwankeri	29.51	-1.58
	Rwerere	29.88	-1.53
	Save	29.76	-2.55
	Shangi	29	-2.38
Shyogwe	29.78	-2.13	
<b>Uganda</b>	Arua	30.92	3.05
	Gulu	32.28	2.78
	Lira	32.9	2.25
	Masindi	31.72	1.68
	Soroti	33.62	1.72
	Tororo	34.17	0.68
	Jinja	33.19	0.45
	Kasese	30.1	0.18
	Mbarara	30.68	-0.6
	Entebbe	32.45	0.05
	Kabale	29.8	-1.22
	Kampala	32.63	0.25

### Reanalysis data

The study considered three long-term gridded datasets as an alternative source over the data scarce region of Central East Africa (CEAF) for comparison and evaluation. They include Climate Hazards Group Infrared Precipitation with Station data (CHIRPS) which is a global rainfall dataset that ranges from 50°S – 50°N and extends from 1981 to present (20), with a spatial resolution of 0.05°\*0.05° and a monthly time scale. The data is available at <https://www.chc.ucsb.edu/data/chirps>. The Climatic Research Unit (CRU TS v4.04) precipitation, a monthly gridded dataset for 1901-2017 at a 0.5° x 0.5° resolution (Harris et al., 2014), the data is available at <https://www.climateurope.eu/datasets-climatic-research-unit-cru/>. Also utilized is the latest version of the Global

Precipitation Climatology Centre (GPCC v8), a monthly precipitation dataset with a period of 1891 to 2016 and a resolution of (0.5° x 0.5°) provided by the World Climate Research Program (WCRP). The data is available at <https://climatedataguide.ucar.edu/climate-data/gpcc-global-precipitation-climatology-centre>. Because the African rain-gauge data has many spatial and temporal discontinuities over large sections of Africa, including the CEAF region, a gridded precipitation dataset is preferred over station data, as pointed out by [21].

## Methods

### Taylor Diagram

Taylor diagram provides a graphical summary of how closely a pattern or set of patterns resembles observations. Taylor diagrams are well-accepted performance metrics for climate models that give a brief statistical outline of how well spatial-temporal patterns match each other in terms of their correlation coefficients (CC) root-mean-square error (RMSE) and the simulated to the observed ratio of their variances. The distance from the origin represents each model's normalized standard deviation (NSD). Using this metric, the model has the largest CC, normalized standard deviation close to the unity (i.e., close to the observation), and smaller RMSE is considered the best among them.

### Empirical Orthogonal Function (EOF)

The empirical orthogonal function (EOF) technique seeks to identify a new set of variables that capture most of the observed variance in the data via a linear combination of the original variable. The EOF is a widely used statistical method to minimize the multidimensionality of complex climate data and identify basic physical modes with a chance of minimum information being lost [22]. Therefore, it is a successful method to draw attention to the physical mechanisms that can potentially contribute to climate variability[23].

The orthogonal function of EOF is defined as follows:

$$z(x, y, t) = \sum_{k=1}^N PC(t) \times EOF(x, y)$$

**Equation 1**

Where  $z(x, y, t)$  denotes the function of space  $(x, y)$  and time  $(t)$ , therefore,  $EOF(x, y)$  represents the spatial structure in relation to temporal variation of  $Z$ . It is more important when discussing “physically meaningful EOFs rather than choosing truncation points. A collection of EOFs presents a convenient orthogonal basis set that is more tailored to the data than those that arise from classical differential equations. On the other hand, if one wants to interpret an individual EOFs in physical terms, it is much more important to be sure that the EOF is not sensitively dependent on the sample. EOF tend to give biased estimates of variance. For instance, the leading EOF is specially designed to explain maximal variance in the available sample. However, the detailed weighting required to achieve this variance is peculiar to the sample and will not consistently hold in independent data sets. As a result, the leading EOF will typically account for less variance in an independent data set than it did in the sample from which it was derived. This reasoning suggests that if bias in variance is an important issue in a particular analysis, EOFs should be used with care.

Empirical orthogonal function (EOF) analysis was used in this study to investigate the dominant modes of variability of the MAM (March-April-May) and OND (October-November-December) rainfall over the region. The data set was normalized to prevent areas (and seasons) of maximum variance from dominating the eigenvectors[24]. The standardized rainfall anomaly  $z$  is computed as expressed in Equation 2

$$z = \frac{x - \bar{x}}{s_d}$$

**Equation 2**

Where the observed MAM and OND rainfall is  $x$ ,  $\bar{x}$  is the long-term mean MAM OND rainfall and  $S_d$  is the MAM-OND rainfall standard deviation. The value of  $z$  provides immediate information about the significance of a particular deviation from the mean [25].

### **Linear Trend Analysis**

To investigate the duration of the tendency and precipitation anomaly over the study area, the Theil–Sen. The slope (TSS) technique was used. This technique is used to calculate the magnitude of the linear trend's slope for the given data. [26] . Because of the robust characteristics of outliers in datasets, this method is thought to be effective. It is unaffected by any extreme distribution and does not imply a typical residual distribution. It has been widely used in various studies to investigate the linear tendencies of hydroclimatic variables across a wide range of domains. It is unaffected by any extreme distribution and does not imply a typical residual distribution.[27-30].

### **Sequential Mann-Kendall Test**

The sequential Mann–Kendall (MK) statistical test was used to detect abrupt changes in rainfall trends [31]. This method has been widely used, especially in climate, environmental, and hydrological studies. It is a valuable tool for comparing any trend in a given time series to the null hypothesis of no trend [32,33]. The sequential MK test used in this study explains the trends and significance of climate parameters and the impact of these changes on water resource management of drought severity.  $U(t)$  and  $U(t)$  represent progressive and retrograde trends for rainfall to demonstrate the changes.

### **Wavelet power spectrum (WPS) analysis**

To characterize the precipitation cycle and possible periodicity, the wavelet transform is used. It demonstrates the completion of the time scale representation of localized frequency information and transient phenomena occurring at various time scales. Torrence and Compo [34] provide detailed information on the equations and features required to apply this technique. The wavelet transform uses a decomposition approach to highlight possible frequencies and signals during the post-processing of datasets. The continuous wavelet transform (CWT) analysis was used in this study to generate varying coefficients that represent the similarity between the signal and mother wavelets at any given scale base. The CWT equation is given below.

## Results and discussion

### Data evaluation and comparison

The Taylor diagram (Taylor 2001) graphically displays how closely pattern(s) from one or more data sets resembles reference data. In this work, each point on the diagram was represented by three statistics: correlation coefficient (indicated by the angle in the polar plot), the ratio of standard deviation normalized by the standard deviation of the observed data (a radial distance of the point from the origin) and unbiased Root Mean Square Different (ubRMSE), distance from the point on the x-axis identified as “Station”). Using this method, the data with the highest correlation, smallest RMSE and closest to the ratio of the reference data, is considered to be the most pertinent data.

Due to the small number of weather stations (48) used in the present study compared to the surface area of AGLR and considering missing data from the various stations, gridded data with the exact temporal resolution was employed as a substitute precipitation dataset. Taylor diagrams of Station, GPCC, and CRU Precipitation dataset were plotted for R1, R2, and R3 as described in Figure3. From the analysis presented, most regions (R1, R2, and R3) had the GPCC performing relatively better than the CRU, with the highest Correlation Coefficient ( $\geq 0.95$ ) and low RMSE ( $\leq 0.5$ ) in all regions.

Through the Taylor diagram [TABLE 3] the CHIRPS dataset may well capture the monthly rainfall pattern compared to both CRU and GPCC, by high correlation coefficient  $r = 0.962$ , low RMSE=16.62, and low bias= 16.62 [TABLE 3]. These results concur with other past researchers [35–38]. In this case, the CHIRPS dataset has the lowest RMSE and bias and the highest correlation coefficient. Therefore, CHIRPS was used in this study for further analysis.

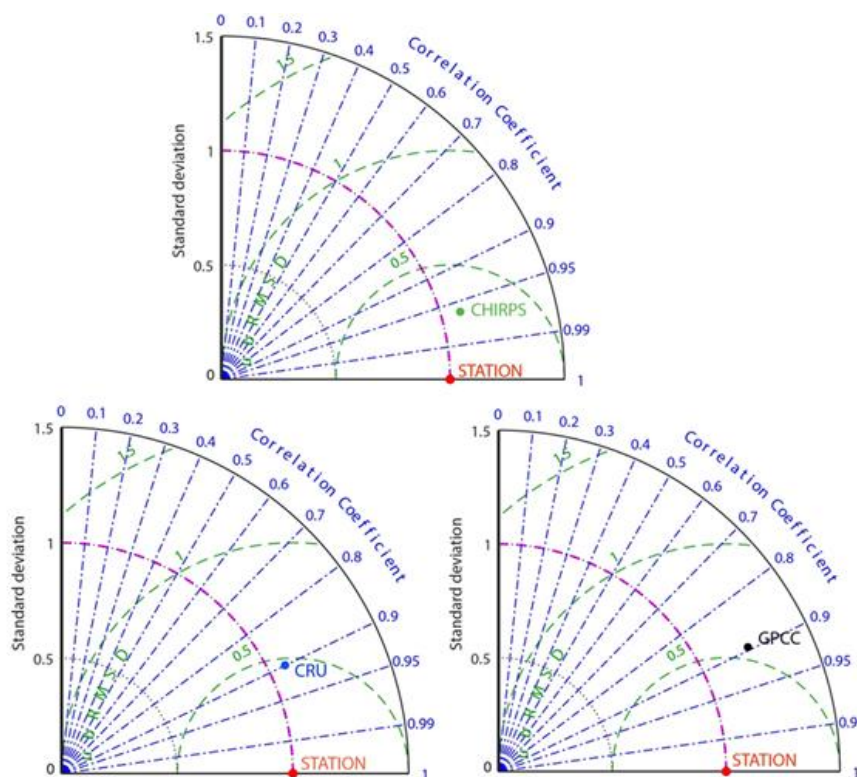


**FIG. 3. Comparison of three gridded monthly rainfall datasets (mm/month) by Taylor diagram technique over CEAF.**

**TABLE 2 Comparison of station data and gridded data sets.**

Data set	Correlation	UbrMSE
CHIRPS	0.962	16.62
CRU	0.89	24.824
GPCC	0.847	28.947

**Rainfall characteristics over CEAF**

The temporal distribution over AGLR was investigated. [FIG.4.]shows an increase in Precipitation from February, reaching its maximum in April, then decreasing again from May, reaching its minimum in June. Another Pick is seen in December, going down to February. The increased amount of Precipitation during March and April is due to the multiple systems: the ITCZ that migrates from South to North and vice-versa. During March and April, it is located in the equatorial line. Another important system is the ENSO, and IOD bringing a high amount of precipitation.

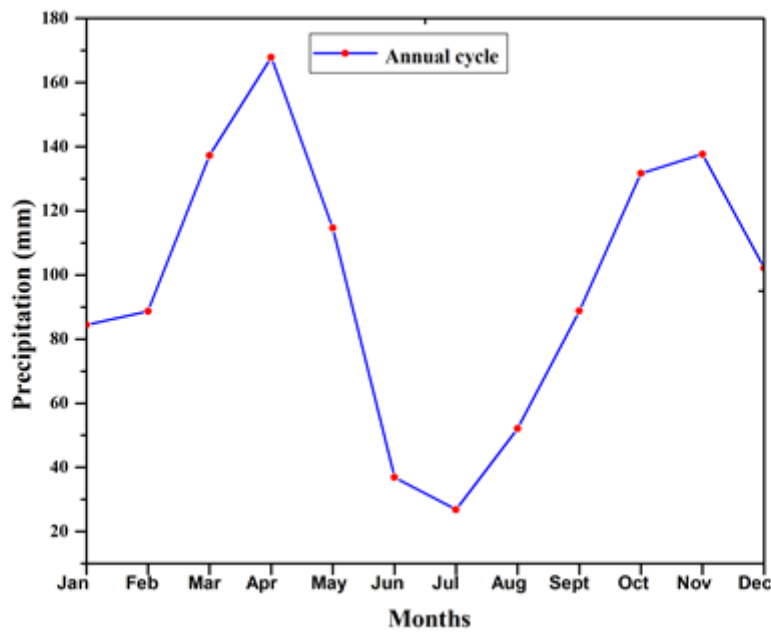


**FIG 4 Temporal distribution of monthly averaged precipitation (mm) over CEAF during 1981-2016.**

The monthly contribution of rainfall from 1981 to 2016 in the area that displays April as the month with the highest amount of rain, followed by March, December, and November. [TABLE 3] showed the seasonal contribution of rainfall, highlighting the driest seasons as well. With a total rainfall of 1235.75 mm, the months of July had the lowest amount of rain during that period, followed by June and August. The mean average of the monthly rainfall distribution, MAM,

OND, JF, and JJAS, contributes about 34.13%, 29.58%, and 16.26%, respectively, the annual total area average of rainfall over AGLR.

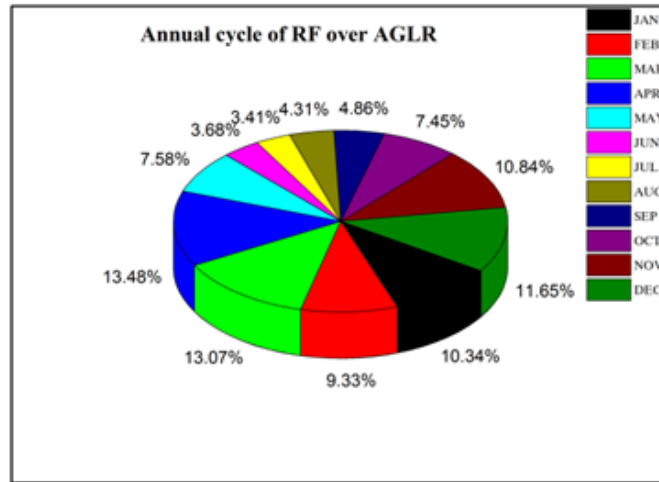


**FIG.5. Monthly contribution of rainfall (%) over AGLR during 1981-2016.**

**TABLE 3 Contribution of seasonal rainfall over AGLR based on GPCC data from 1981-2016.**

SEASONS	TOTAL RF (mm)	% of Total Annual RF
JF	189.62	8.8%
<b>MAM</b>	<b>420.49</b>	<b>39.64%</b>
JJAS	236.99	22.7%
<b>OND</b>	<b>388.62</b>	<b>28.8%</b>
Annual Total	1235.72	99.94%

**Precipitation Modes over AGLR (EOF Results)**

Empirical Orthogonal Function (EOF) helps determine several functions that describe most of the data’s variance by defining dominant mode using eigenvectors. Since the eigenvector with the largest eigenvalue of the covariance matrix is referred to as the leading EOF and the eigenvector associated with the second largest eigenvalue of the covariance matrix is referred to as the second EOF and so on. The analyses of EOF were to determine the dominant mode responsible for rainfall over AGLR in the two rainy seasons of MAM and OND.

The spatial vectors and the corresponding time series of the three EOF modes analyzed in this study during the first season (OND)[FIG.6.]. The percentage variability of the first, second, and third modes is 60.64%, 11.15%, and 5.14%. The three EOF modes revealed different precipitation patterns. The first EOF shows a bimodal regime of variability over the region with positive loadings all over the area. The second EOF offers a dipole mode of variability with negative loadings in the North-Eastern part and positive loadings in the South and Northwestern part of the region. The third EOF

shows a dipole mode of variability over the area with negative loadings in the region’s eastern part. The Northern and central to the west part are covered with positive loadings, and the Southwestern part.

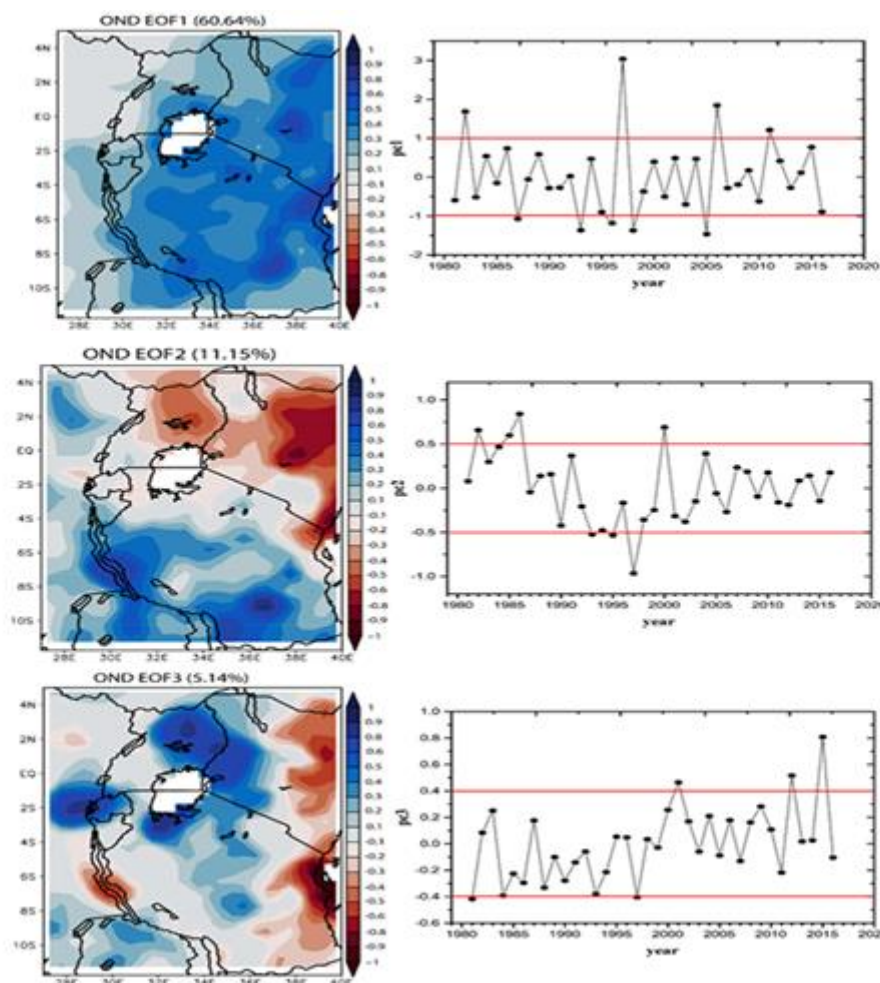


**FIG. 6. the first three modes for the OND rainfall anomaly showing spatial distribution (left) and their corresponding principal components (right) over CEAF from 1981-2016.**

**Long-Term Monotonic Trends for Precipitation**

**Seasonal and Annual Precipitation Trends Over time**

The results for temporal variations and seasonal and annual trends precipitation over CEAF are presented in [FIG.7.] The time-series results were obtained by averaging the rainfall using the CHIRPS rainfall datasets. The precipitation over the study domain is generally declining with a negative slope in both scenarios. Throughout the study period, the year 1997 recorded the maximum annual rainfall, with a mean value of about 1220.431 mm, and the lowest amount of rain was received in 2005 with a mean value of only 872.9785 mm.

The trends were computed using the Theil–Sen Slope method. The results clearly show positive changes in the 1980s and 1990s, followed by a negative change in the 2000s. Over the study area, annual rainfall showed a positive trend. Furthermore, during the 1999–2008 decade, the years of 1997 and 2005 witnessed the highest increase and decline in rainfall. Studies conducted by numerous researchers concur with the present study’s findings, both connected to the

oceanic drivers in the western Indian Ocean and central-eastern Pacific Ocean, hence the positive episodes of ENSO and IOD.

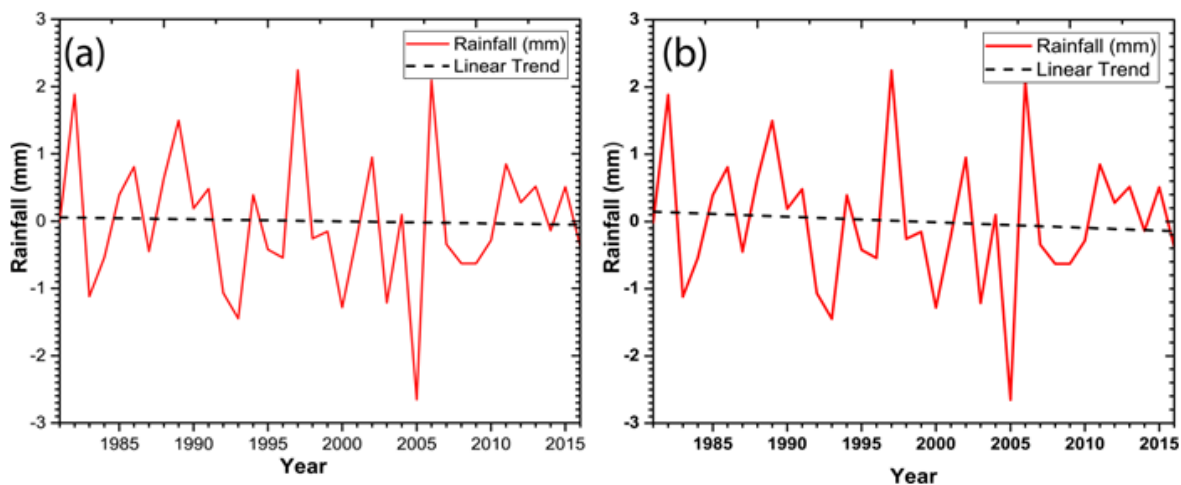


**FIG.7. Time series of (a) seasonal and (b) annual rainfall over CEAf from 1981 to 2016.**

### Sequential Mann Kendall

The present study employed the Mann–Kendall trend test to detect the possible significant and abrupt changes in rainfall patterns over the study area from 1981 to 2019. The annual and OND time series results show a Z score of -0.2770 and 0.0136 [TABLE 4] below the threshold value of 1.96, signifying slight positive tendencies. However, the variance (S) shows negative values for interannual and positive values for OND season, indicating a reduction in rainfall at the interannual timescale against a slight increase in precipitation at the seasonal timescale. [FIG.8.] shows results for sequential Mann–Kendall statistic values of progressive  $u(t)$  (solid black line) and retrogressive  $u'(t)$  (red dotted line), derived from CHIRPS precipitation datasets for OND, and annual mean over CEAf during 1981–2016 period.

The analysis demonstrates an insignificant positive trend during the short rains season and an insignificant negative trend based on the inter-annual scale. As highlighted in Figure 8 for both annual and OND season. For instance, on the interannual time scale, there was a slight decrease in rainfall at the beginning of the study period (1981), followed as the progressive and retrograde curves intersected three times between 1981 and 1985. On the other hand, the seasonal trend shows a slight increase in rainfall at the beginning and no significant changes in amplitude in the first five years. However, the seasonal trend shows an abrupt negative change from 1985 to almost the end of the study period, while for the interannual trend, there is no apparent change.

These fluctuations can be based on the fluctuations in water resources, especially the decline in the primary water bodies levels such as Lakes Victoria and Tanganyika, resulting from climate change [39]. The decreasing trend in OND total rainfall impacted negatively by reducing the number of wet days, thereby affecting the cropping cycle and maturity of staple foods.

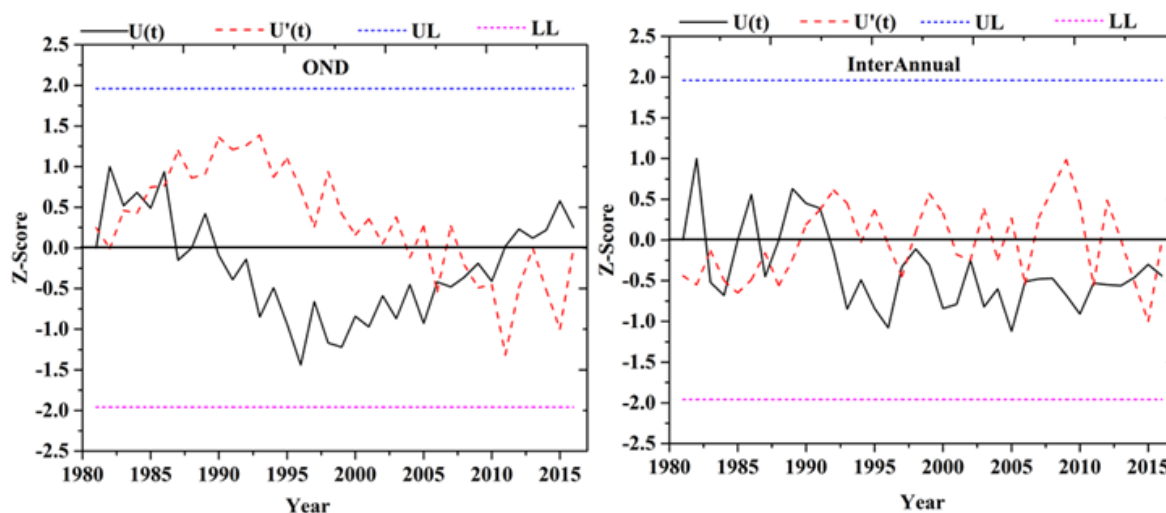


**FIG. 8.** Abrupt changes of seasonal (left) and annual (right) precipitations over CEAF.  $u(t)$  is progressive sequential while  $u'(t)$  is retrogressive sequential statistics. The blue and red dashed lines corresponding to  $\pm 1.96$  at 0.05 confidence level.

**TABLE 4** Summary of MK results for annual and seasonal rainfalls over CEAF during 1981–2016.

Trend Analysis	MK Rainfall (mm)	
	Annual Rainfall	Seasonal Rainfall
Mean (mm/month)	88.43	105.81
Slope	-0.0226	0.0017
Z-score	-0.2770	0.0136
P-value	0.7818	0.9891
$\alpha$	0.05	0.05
Significance	Insignificant decreasing trend	Insignificant increasing trend

**Wavelet power spectrum analysis of rainfall changes**

It depicts the OND rainfall time series and the corresponding wavelet power spectrum (WPS). The black contour lines in the WPS represent regions with greater than a 95% confidence level in relation to the red noise background spectrum[FIG.9.]. The solid curve delineates the “cone of influence,” which accounts for edge effects. As a result, the results in this region should be viewed with caution. As a result, results in this region should be interpreted with caution because they may be less accurate. It’s worth noting that Figure 9b shows a 1-year band as the dominant period of variability, which is typical of annual mean precipitation. The 1-2 year band extends from the start of the time series to around 2014, near the end of the time series (1981–2016). It is also worth noting. Also, the 1-2year band contains several instances of significant periodicity enclosed by contours greater than the 95 percent confidence level. When the signals are localised in the study region, the years are primarily known to be wet years, which include 1996, 1997, 1998, 2002, 2006, and 2015. The results concur with the results found in the first principal component.

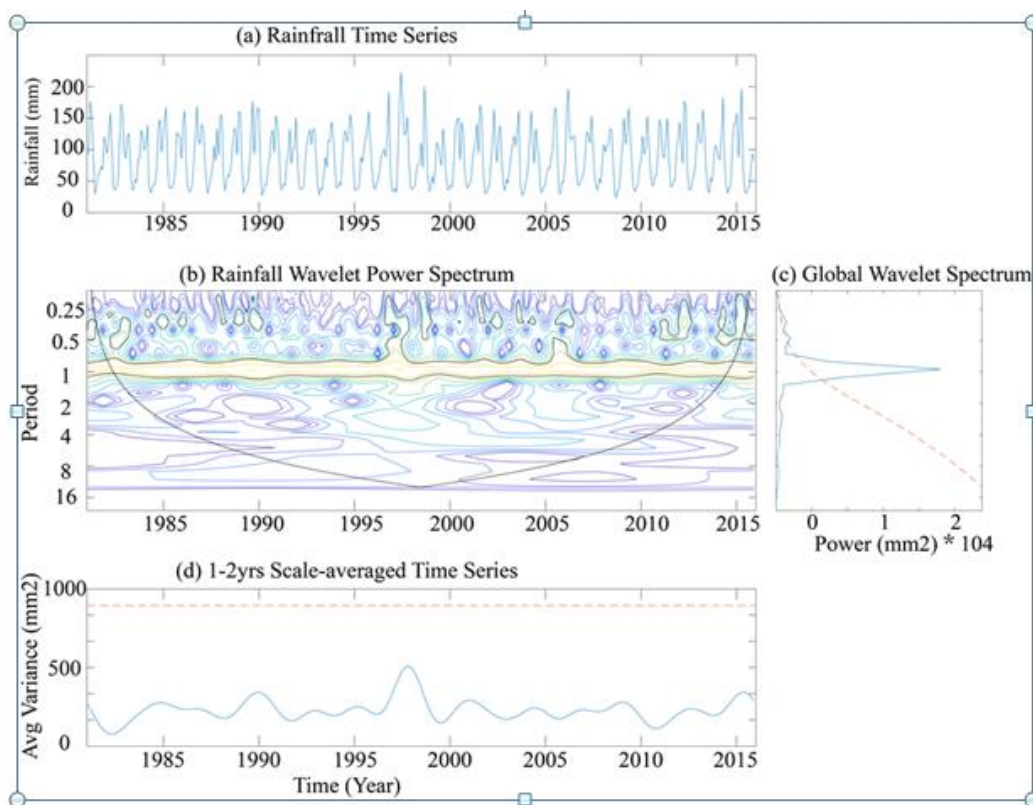


**FIG.9. (a) Time series of the Precipitation over CEAF ; (b) Rainfall wavelet power spectrum; (c) Global Wavelet Spectrum ( red dashed line is at 5% significance level); (d) 1–2-year scale averaged time series,the dashed line indicates passing the 0.05 confidence level.**

### Conclusions

Specific objectives guided the present study on the characteristics of spatial and temporal trends and periodicities over CEAF from 1981 to 2016: Analyze the spatial-temporal distribution of seasonal and annual rainfall variability in Central East Africa (CEAF) through statistical metrics such as correlation analysis, linear trends, sequential Mann-Kendal and empirical orthogonal function. During this study, several points helped us reach the conclusions:

The first point of the study was to compare the reanalysis data CHIRPS, CRU and GPCC. The study results showed that CHIRPS data performed better over CRU and GPCC datasets, leading me to use CHIRPS datasets for further analysis. The second point was to study the climatology of the region and then decide on the rainfall seasons. Results showed a bimodal rainfall regime over the study area where we encountered two rainfall seasons (long and short), MAM and OND, respectively. The Third point of the study involved using the reanalysis datasets (CHIRPS) to analyze the spatial-temporal rainfall distribution over the study area from 1981 to 2016. Results from EOF explain a 60% variability during the short rainy season (OND). The results revealed the interannual variability through the principal components of the dominant EOF mode [FIG.6.] the extreme years (wet and dry) years of the short rainy season.

The second point tackled in this study is the trend analysis through a series of robust techniques such as the sequential Mann-Kendall (SQMK) and the wavelet power spectrum (WPS) analysis. The first method revealed a set of statistics used to interpretate the state of the trend on the seasonal and interannual time scales. Generally, there is an increase in



11. Nicholson SE. Climate and climatic variability of rainfall over eastern Africa. *Rev Geophys*. 2017.
12. Lüdecke HJ, Müller-Plath G, Wallace MG, Lüning S. Decadal and multidecadal natural variability of African rainfall. *J Hydrol Reg Stud*. 2021.
13. Limbu PTS, Guirong T. Relationship between the October-December rainfall in Tanzania and the Walker circulation cell over the Indian Ocean. *Meteorol Zeitschrift*. 2019;28.
14. King JA, Washington R, Engelstaedter S. Representation of the Indian Ocean Walker circulation in climate models and links to Kenyan rainfall. *Int J Climatol*. 2021;41.
15. Zhao S, Cook KH. Influence of Walker circulations on East African rainfall. *Clim Dyn* [Internet]. 2021.
16. Hastenrath S, Polzin D, Mutai C. Circulation mechanisms of Kenya rainfall anomalies. *J Clim*. 2011;24.
17. Dyer ELE, Jones DBA, Nusbaumer J, et al. Congo Basin precipitation: Assessing seasonality, regional interactions, and sources of moisture. *J Geophys Res*. 2017;122.
18. Munday C, Washington R, Hart N. African Low-Level Jets and Their Importance for Water Vapor Transport and Rainfall. *Geophys Res Lett*. 2021;48.
19. Owiti Z, Zhu W. Spatial distribution of rainfall seasonality over East Africa. *J Geogr Reg Plan*. 2012.
20. Funk C, Verdin A, Michaelsen J, Peterson P, Pedreros D, Husak G. A global satellite-assisted precipitation climatology. 2015.
21. Iii CJS, Semazzi FHM. Variability of the recent climate of eastern Africa. 2004.
22. Jolliffe IT. *Principal Component Analysis*, Second Edition. 2002. 21.
23. Dommengot D, Latif M. A cautionary note on the interpretation of EOFs. *J Clim*. 2002;15(2):216–25.
24. Koumare I. Temporal / Spatial Distribution of Rainfall and the Associated Circulation Anomalies over West Africa. *Pakistan J Meteorol*. 2014.
25. Kabanda T. Long-Term Rainfall Trends over the Tanzania Coast. *Atmosphere (Basel)*. 2018..
26. Pranab kumar sen. Estimates of the regression coefficient based on Kendall's tau\* estimates of the regression coefficient based on Kendall's tau\*. 2013..
27. Ongoma V, Haishan C, George OW. Variability of Extreme Weather Events over the Equatorial East Africa, a case study of Rainfall in Kenya and Uganda Variability of extreme weather events over the equatorial East Africa, a case study of rainfall in Kenya and Uganda. *Theor Appl Climatol*. 2016.
28. Mumo L, Yu J, Ayugi B. Evaluation of spatiotemporal variability of rainfall over Kenya from 1979 to 2017. *J Atmos Solar-Terrestrial Phys* [Internet]. 2019.194.
29. Mumo L, Yu J, Fang K. Assessing Impacts of Seasonal Climate Variability on Maize Yield in Kenya. *Int J Plant Prod*. 2018
30. Wang G, Gong T, Lu J, et al. On the long-term changes of drought over China (1948–2012) from different methods of potential evapotranspiration estimations. *Int J Climatol*. 2018..
31. B.Mann H. *Nonparametric Tests Against Trend*. Econom Soc. 2013.
32. Araghi A, Mousavi-Baygi M, Adamowski J. Detection of trends in days with extreme temperatures in Iran from 1961 to 2010. *Theor Appl Climatol*. 2016.125.
33. Ayugi B, Tan G, Gnitou GT, Ojara M, Ongoma V. Historical evaluations and simulations of Precipitation over East Africa from Rossby centre regional climate model. *Atmos Res* [Internet]. 2020.
34. Torrence C., Compo G. A practical guide to wavelet analysis. *Bull Am Meteorol Soc*. 1998;79.
35. Cattani E, Merino A, Guijarro JA, Levizzani V. East Africa Rainfall trends and variability 1983-2015 using three long-term satellite products. *Remote Sens*. 2018..
36. Dinku T, Funk C, Peterson P, Maidment R, Tadesse T. Validation of the CHIRPS satellite rainfall estimates over eastern. 2018.
37. Nkuzimana A, Bi S, Abdallah M, Alriah A. Comparative Analysis of the Performance of Satellite - Based Rainfall Products Over Various Topographical Unities in Central East Africa : Case of Burundi. 2020.
38. Seregina LS, Pinto JG, Fink AH. A new and flexible rainy season definition : Validation for the Greater Horn of Africa and application to rainfall trends. 2018.
39. Sutcliffe J V., Petersen G. Lake Victoria: Derivation of a corrected natural water level series. *Hydrol Sci J*. 2007.